Author Manuscript
Author Manuscript
Author Manuscript
Author Manuscript

HHS Public Access
Author manuscript
Bioconjug Chem. Author manuscript; available in PMC 2019 June 04.

Published in final edited form as:
Bioconjug Chem. 2018 November 21; 29(11): 3776–3782. doi:10.1021/acs.bioconjchem.8b00640.

Nanoemulsion-Based Delivery of Fluorescent PARP Inhibitors in Mouse Models of Small Cell Lung Cancer

Junior Gonzales[†], **Susanne Kossatz**[†], **Sheryl Roberts**[†], **Giacomo Pirovano**[†], **Christian Brand**[†], **Carlos Pérez-Medina**[‡], **Patrick Donabedian**[†], **M. Jason de la Cruz**[⊥], **Willem J. M. Mulder**[‡,§], and **Thomas Reiner**[*,†,‖]

[†]Department of Radiology, Memorial Sloan Kettering Cancer Center, New York, New York 10065, United States [‡]Translational and Molecular Imaging Institute, Department of Radiology, Icahn School of Medicine at Mount Sinai, New York, New York 10029, United States [§]Laboratory of Chemical Biology, Department of Biomedical Engineering and Institute for Complex Molecular Systems, Eindhoven University of Technology, Eindhoven, The Netherlands [⊥]Structural Biology Program, Sloan Kettering Institute, Memorial Sloan Kettering Cancer Center, New York, New York 10065, United States [‖]Department of Radiology, Weill Cornell Medical College, New York, New York 10065, United States

Abstract

The preclinical potential of many diagnostic and therapeutic small molecules is limited by their rapid washout kinetics and consequently modest pharmacological performances. In several cases, these could be improved by loading the small molecules into nanoparticulates, improving blood half-life, *in vivo* uptake and overall pharmacodynamics. In this study, we report a nanoemulsion (NE) encapsulated form of PARPi-FL. As a proof of concept, we used PARPi-FL, which is a fluorescently labeled sensor for olaparib, a FDA-approved small molecule inhibitor of the nuclear enzyme poly(ADP-ribose)polymerase 1 (PARP1). Encapsulated PARPi-FL showed increased blood half-life, and delineated subcutaneous xenografts of small cell lung cancer (SCLC), a fast-progressing disease where effcient treatment options remain an unmet clinical need. Our study demonstrates an effective method for expanding the circulation time of a fluorescent PARP inhibitor, highlighting the pharmacokinetic benefits of nanoemulsions as nanocarriers and confirming the value of PARPi-FL as an imaging agent targeting PARP1 in small cell lung cancer.

Graphical Abstract

[*]**Corresponding Author:** reinert@mskcc.org.

Supporting Information
The Supporting Information is available free of charge on the ACS Publications website at DOI: 10.1021/acs.bioconjchem.8b00640. Detailed characterization of PARPI-FL NE, H-82 tumors, and epifluorescence images, cryo-TEM images, table with physical features of PARPi-FL NE and PARPi-FL, microscopy images of excised H-69 and H-82 tumor xenografts from different sections (PDF)

Author Manuscript Author Manuscript Author Manuscript Author Manuscript

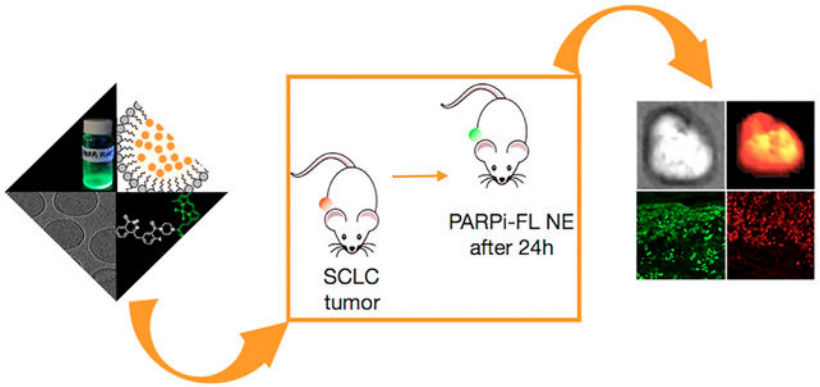

INTRODUCTION

Although the diagnosis and treatment of certain types of cancers has seen significant improvements in recent decades, advances in treatment of other, more recalcitrant cancers remain an unmet clinical need. This is particularly true for small cell lung cancer (SCLC), a subset of the general lung cancer population (13%, 29000 of 221000 patients in the U.S. annually).[1] SCLC is one of the deadliest types of malignant growth, and its mortality far exceeds those with more societal presence, such as leukemia, colorectal cancer, melanoma, breast, and prostate cancers.[2] Annually, 27000 patients perish from SCLC in the U.S., only slightly less than from prostate and breast cancer (29430 and 41400 patients, respectively). PARP inhibitors (PARPi) are currently under investigation as a treatment option for SCLC, in combination with chemo- or radiotherapy.[3–7] PARPi exert their therapeutic properties by disruption of the single-stranded DNA-damage repair pathway regulated by PARP1.[8–10]

In the past, small molecules have been formulated as nanoparticulate systems, resulting in better delivery, reduced off-target effects, and overall better pharmacokinetics and dynamics.[11] It is with this in mind that we explored the encapsulation of PARP inhibitors, a class of compounds that can be used for traditional therapy[8,9,12] but also imaging[10,13] and radiotherapy.[14–17]

Whereas many PARP inhibitors have a high affinity and specificity, they feature poor solubilities and short blood half-lives, reducing the resulting tumor uptake. We hypothesized that a nanoformulated, fluorescently labeled PARP inhibitor would increase uptake in tumors by expanding the circulation time, whereas intratumoral release would retain specific target binding and retention of the inhibitor itself.

As a fluorescent PARP inhibitor, we chose PARPi-FL (Figure 1a), a well-characterized small molecule that was used in several investigations before.[18–20] The hydrophobicity of PARPi-FL makes the targeted tracer an ideal candidate for encapsulation in nanoemulsions, heterogeneous liquid-in-liquid droplets of about 50–200 nm in diameter.[21] Nanoemulsions (Figure 1b) are excellent shuttles for the delivery of payloads at different and later time points in comparison to small molecule imaging agents.[22,23] The makeup of the nanoformulation was selected based on previously completed studies.[23,24] In essence,

Author Manuscript Author Manuscript Author Manuscript Author Manuscript

nanoformulations are small droplets of oil, stabilized by lipids, cholesterol, DSPC, and DSPEPEG2000.

Our central hypothesis was that PARPi-FL nanoemulsions would be capable of delivering fluorescent PARPi-FL to SCLC tumor cells by first enabling delivery of the small molecule to the tumor via the enhanced permeation and retention (EPR) effect,[25] followed by a release of the small molecule and the subsequent uptake by PARP1-expressing tumor cells. Consequently, our expectation was to observe some nuclear staining after PARPi-FL nanoemulsion (PARPi-FL NE) was injected. We tested a PARPi-FL NE in H-69 and H-82 xenograft mouse models of SCLC, confirming the ability to demarcate SCLC with high contrast after intravenous administration. This novel application allowed PARPi-FL to be delivered to the malignant tissue with favorable biodistributions and pharmacokinetics, which might represent a particularly elegant way to site-selectively deliver low-range radiopharmaceuticals like Auger emitters.[26,27] We believe that a PARPi-FL NE could represent a first step toward designing new nanoparticulate PARP inhibitor platforms for imaging and therapy.

RESULTS AND DISCUSSION

We determined the retention times of PARPi-FL and PARPi-FL NE using size-exclusion chromatography (SEC) (20 and 11 min, respectively, Figures 1c and 1d). Using dynamic light scattering (DLS), we found that the PARPi-FL NE had a minimum effective diameter of 144 nm and maximum effective diameter of 157 nm (Figure S1a) with an average particle system concentration of 1.3 nM, a ζ-potential of −6.03, and a polydispersity index (PDI) of ≤0.17. These physical features are also summarized in Table S1. After synthesis and purification, 300 μL of the nanoemulsion was lyophilized, redissolved in dimethyl sulfoxide (DMSO), and extracted to estimate the amount of PARPi-FL present inside the nanoemulsion. The diameter of our nanoemulsions was larger in comparison to what we have reported in the past with other nanoemulsion preparations but still comparable with sizes reported in the field.[24,28] This was also corroborated by cryo-TEM (Figure S1b), which showed that PARPi-FL NE had a heterogeneous morphology. The negative ζ-potential can be attributed to the ethers, making up large components of PEG2000 which are useful to improve the pharmacokinetics.[29,30]

PARPi-FL NE was formulated by adapting a previously described method, using stirring alone, which could be an important asset when loading radiotherapeutically labeled PARP1 inhibitors, allowing encapsulation of radionuclides in a more efficient and safer manner, avoiding sonication—and potential aerosolization—of the radioactive materials.[31] Similarly, nanoemulsions can increase overall delivery and internalization of PARPi, shielding them from being delivered to healthy, PARP-expressing cells, including components of the blood or bone marrow.[32–35] Similar work was performed with nonlabeled talazoparib, a poorly soluble but potent PARP inhibitor, which has been encapsulated in nanoemulsions for therapy of breast and pancreatic cancer. Although encapsulated talazoparib showed increased drug accumulation and apoptosis in comparison to the use of talazoparib alone, no visualization of release or internalization was observed due to the lack of an imaging moiety.[36]

Author Manuscript Author Manuscript Author Manuscript Author Manuscript

We used two orthogonal methods to estimate the encapsulation efficacy (EE). First, the EE was calculated from lysing the nanoemulsion (Figures S1c and S2a) and analyzed for free PARPi-FL molecules using a PARPi-FL calibration curve. Second, the EE was also calculated from a collected filtrate using the KrosFlo tangential flow filtration system and quantified nonincorporated PARPi-FL (Figure S2b). The EE was measured to be 22 ± 1.2% and 23 ± 3.3% for KrosFlo and re-extraction (Figure S2c), respectively. In line with the characterization, a nanoparticle tracking analysis provided us with an estimated idea of the nanoemulsion particle concentration, which was found to be 1.3 nM. Taken together, we tuned our preparation so that each formulation run of the nanoemulsion yielded approximately 50 μg or 78 nmol of incorporated PARPi-FL. Formulations were combined and concentrated down for final administration. We started this task by lysing 300 μL of PARPi-FL NE, which upon extraction of the PARPi-FL based on the calibration curve (Figures S3a and S3b) had a concentration of 30 ± 3.3 μM. With the aforementioned particle concentration of 1.3 nM, this suggests that about 2×10^4 molecules of PARPi-FL are contained in each nanoemulsion.

Additionally, we determined the stability of the encapsulated PARPi-FL NE. This was done by washing the nanoemulsion in a spin column six times over a period of 2 h for the first day and twice a day for the next 2 days. After each wash, a fluorescence measurement was taken to detect the presence of PARPi-FL, and no leached PARPi-FL was observed in the collected washes (Figure S3c). Our formulation also shows high stability in human serum. Using SEC, we demonstrated that our nanoemulsion showed little (<5%) or no change over a period of 24 h, and that most of the nanoemulsion remains intact (Figures 2a and 2b). A similar pattern was observed for the nanoemulsion in PBS (pH 7.4) at 37°C. To validate the performance of PARPi-FL NE in vivo, we used the human SCLC xenograft models H-69 and H-82. The blood half-life of the PARPi-FL NE was approximately 6 h (Figure 2c). After 48 h, PARPi-FL NE had washed out from the blood, in line with the expected pharmacokinetics. This represents a significantly expanded blood half-life showing a longer circulation in comparison to the non-encapsulated fluorescent small molecule (24.5 min).[18] We first confirmed the presence of PARP1 in both H-69 and H-82 tumors via Western blots, whereas only negligible expression was detected in the lung and brain (Figure 3a). H-69 and H-82 tumor-bearing mice were divided into three groups (≥3 mice per group, Figure S4). Cohort 1 was a negative control, and cohort 2 was injected with 200 μL of PARPi-FL NE (0.39 mM, 78 nmol of PARPi-FL in 200 μL of PBS). Cohort 3 (block) was injected with 100 μL of olaparib solution (23 mM, 4.6 μmol in 200 μL of PBS with 30% PEG300, 20% DMSO) 45 min before and 18 h after the PARPi-FL NE injection (0.39 mM, 78 nmol of PARPi-FL in 200 μL of PBS).

Epifluorescence imaging of excised subcutaneous H-69 and H-82 tumors was performed 24 h after injection of PARPi-FL NE and post mortem for control mice. The intensity of the fluorescence signal was compared to that of thigh muscle tissue, spleen, and lung tissues. PARPi-FL NE generated a strong fluorescence signal in tumors and almost no fluorescence in other organ tissues (Figures 3b and S5a,b). We were able to confirm the specificity of accumulation by blocking of PARP1 binding sites with the nonfluorescent PARP1 inhibitor olaparib before administration of the PARPi-FL NE, which resulted in an almost total block of the fluorescence signal of the tumor, reducing the average radiant efficiency from 2.3 ×

Author Manuscript Author Manuscript Author Manuscript Author Manuscript

10^7 (PARPi-FL NE) to 2.7×10^6 (olaparib/PARPi-FL NE), $P < 0.001$ (Figure 3c). In control mice, the fluorescence signals did not exceed an average radiant efficiency of 0.7×10^6 in either tumor or muscle. Microscopic analysis of the fluorescence distribution in 10 μm cryosections of the excised tumors revealed both nuclear and perinuclear staining. This suggests the release of PARPi-FL from the nanoemulsion and subsequent specific accumulation of PARPi-FL NE in tumor cell nuclei. Nuclear fluorescence was only observed in H-69 and H-82 tumors when PARPi-FL NE was injected without preinjection of olaparib (Figure 3d and Figures S6 and S7). PARP1 expression was also confirmed using immunofluorescence microscopy (Figures 4 and S8), where similar staining patterns were observed for PARPi-FL NE and anti-PARP1 immunohistochemistry. This suggests that the nanoemulsions are not just delivered macroscopically, but that PARPi-FL can escape the nanomaterial and engages PARP1 inside of cell nuclei. The prepared nanoemulsions were well-tolerated by the animals, and no evidence of toxicity was detected after the injections.

CONCLUSION

In this work, we show the design and validation of a nanoparticulate form of a fluorescent PARP1 imaging agent, PARPi-FL, which was encapsulated in a nanoemulsion. We show that this nanoemulsion accumulates in H-69 and H-82 SCLC tumors, where the imaging agent escapes and localizes to its target in cell nuclei. Importantly, the preparation of these nanoemulsions could be applied and extended to other types of small molecules including other PARP inhibitors. Intuitively, one possible trajectory could be their use to encapsulate radiotherapeutically labeled PARP inhibitors. This would be particularly effective for Auger emitters, which would be shielded in the bloodstream. However, once in the tumor, they would translocate to the nucleus, bind to PARP1, and release their radioactive payloads. This could, ultimately, enhance therapeutic responses while decreasing off-target effects.

EXPERIMENTAL SECTION

General.

Unless otherwise stated, all solvents and reagents were obtained from Sigma-Aldrich and used without further purification. BODIPY-FL was purchased from Invitrogen (Carlsbad, CA). PARPi-FL was synthesized according to methods described previously.[18,20] All high-performance liquid chromatography (HPLC) purifications were performed on a Shimadzu HPLC system equipped with a DGU-20A degasser, a SPD-M20A UV detector, a LC-20AB pump system, a CBM-20A communication BUS module, and a RF-20A xs fluorescence detector (excitation = 498 nm, emission = 510 nm) using reversed-phase columns. SEC experiments were performed on a Superdex 10/300 column with PBS as eluent at a flow rate of 1 mL/min, where both absorbance and fluorescence were recorded. Phospholipids were purchased from Avanti Polar Lipids (Alabaster, AL, USA). Matrigel was purchased from Fisher Scientific. Cell culture media were prepared by the MSKCC Media Preparation Facility. All animals were purchased from Charles River Laboratories, NY, USA. The 2.5% goat serum was purchased from Vector Laboratories. Primary antibody: rabbit anti-PARP1 (sc-7150, Santa Cruz). Secondary antibody: AlexaFluor 568 goat anti-rabbit antibody (A21076, Molecular Probes). Cryo-TEM data were obtained using a using a Thermo Fisher

Author Manuscript Author Manuscript Author Manuscript Author Manuscript

Titan Krios G2 transmission electron microscope operating at 300 kV with Gatan K2 Summit detector.

Preparation of PARPi-FL NE.

PARPi-FL was dissolved in ethanol and diluted to a concentration of 2.26 mM. Mixed lipids, DSPC, cholesterol, and DSPE-PEG2000 (62:33:5 mol ratio) were combined in ethanol to afford 25 mg/mL. One hundred fifty microliters of PARPi-FL from the stock solution (2.26 mM of PARPi-FL in ethanol) was mixed with MCT (miglyol 812 N, Oleochemicals, IOI group GmbH, Germany), and the mixture was added to the lipid solution at a weight ratio of 0.57:1:0.01 lipid/oil/PARPi-FL. The nanoemulsion was synthesized by swiftly injecting 1 mL of this ethanolic mixture into 20 mL of PBS, and the mixture was stirred at 1400 rpm for 13 min. The resulting nanoemulsion was purified through a first centrifugation using 4000 rpm at 22°C for 30 min to remove possible aggregates and then washed at least three times with fresh PBS using 100 kDa molecular weight cutoff (MWCO) centrifugal concentrators (centrifugal viva spin) and finally concentrated using a KrosFlo Research Il Tangential flow filtration system fitted with a mPES Micro-Kross module (100 kDa MWCO, 20 cm^3). This instrument was used to reduce the volume down to approximately 2500 μL. If necessary, a 100 kDa MWCO centrifugal viva spin was used for further washing steps and reducing volumes. The formulation was passed through a PES syringe filter (0.22 μm, 13 mm diameter, Celltreat Scientific Products, Pepperell, MA) before characterization or administration.

Characterization of PARPi-FL NE.

Absorption and fluorescence spectra were measured in a 96-well plate (Corning Costar black clear bottom, Thermo Fisher Scientific) with path lengths of 0.231 and 0.300 cm for volumes of 75 and 100 μL, respectively. UV/vis absorbance and fluorescence spectra were measured on a SpectraMax M5 Multi-Mode microplate reader. Samples were measured together with DMSO in a matched well and volume. Measurements were recorded in triplicates at 25°C. The absorbance scan was performed with an integration time of 0.5 s and a range from 350 to 900 nm in 5 nm steps. The encapsulation efficiency of PARPi-FL in the nanoemulsion solution was determined by re-extracting the PARPi-FL. For this, the nanoemulsions were lyophilized (FreeZone 2.5 Plus, Labconco, Kansas City, MO, USA) and redissolved in DMSO. Extracted PARPi-FL molecules were passed through a PES syringe filter (0.22 μm, 13 mm diameter, Celltreat Scientific Products, Pepperell, MA) before its UV/vis absorption was measured. Using a PARPi-FL calibration curve, the unknown concentrations of the encapsulated PARPi-FL were determined. The size distribution and ζ-potential of the nanoemulsions were determined by dynamic and electrophoric light scattering on a Malvern Zetasizer (Malvern Instrument Ltd., UK). The nanoemulsion concentration was determined using nano-particle tracking analysis (NanoSight Ltd., UK). A size exclusion HPLC of the nanoemulsions was performed using a Superdex 10/300 column (GE Healthcare Life Sciences, Pittsburgh, PA) with PBS as eluent. Cryo-TEM data were obtained following a method previously described.[28] CryoEM drift-corrected imaging was performed at the MSK Structural Biology EM facility using a Thermo Fisher Titan Krios G2 transmission electron microscope operating at 300 kV with Gatan K2 Summit detector, at a nominal magnification of 18000× (super-resolution pixel

Author Manuscript Author Manuscript Author Manuscript Author Manuscript

size of 0.677 Å/pixel). Images were collected at 4 s per exposure, with an electron dose rate of 10 electrons/pixel/s.

Cell Lines.

All cell lines used in this study were obtained from the American Type Culture Collection and grown under aseptic conditions in an incubator providing a humidified atmosphere of 5% CO_2 in air. H-69 and H-82 small cell lung cancer cell lines were used between 18 and 26 passages after thawing to ensure complete revival. H-82 and H-69 cells were cultured in RPMI media supplemented with 10% fetal bovine serum, 2 mM/L glutamine, 10 mM HEPES, 1 mM sodium pyruvate, 4500 mg/L glucose, 1500 mg/L sodium bicarbonate, 100 U/mL penicillin, and 100 μg/mL streptomycin.

Stability of PARPi-FL NE in Human Serum.

Human serum was purchased from Thermo Fisher Scientific. PARPi-FL NE was incubated in human serum (25% nanoemulsion and 75% of serum to get a final volume of 1 mL) at 37°C over a period of 24 h. Fifty microliters of the NE−serum mixture was taken at different time points (1, 2, 4, 6, 12, and 24 h). The samples were analyzed on a Shimadzu HPLC equipped with a SPD-M20A UV detector, a LC-20AB pump system, a CBM-20A communication BUS module, and a RF-20A xs fluorescence detector (excitation = 498 nm, emission = 510 nm). SEC experiments were performed on a Superdex 10/300 column (GE Healthcare Life Sciences, Pittsburgh, PA) using PBS as eluent at a flow rate of 1 mL/min, where both absorbance and fluorescence were recorded.

Stability Experiment of PARPi-FL NE in PBS.

PARPi-FL NE was incubated in PBS at 37°C over a period of 24 h. Fifty microliters of the nanoemulsion was taken at different time points (1, 2, 4, 6, 12, and 24 h). The samples were analyzed on a Shimadzu HPLC using PBS as eluent at a flow rate of 1 mL/min, where both absorbance and fluorescence were recorded.

Blood Half-Life of PARPi-FL NE.

Mice (n = 3) were injected through the tail vein with the PARPi-FL NE system (0.39 mM, 78 nmol of PARPi-FL in 200 μL of PBS). At different time points after injection (5 min, 20 min, 1 h, 3 h, 6 h, 12 h, 24 h, and 48 h), blood was collected via retro-orbital eye bleed or terminal heart puncture. Forty to sixty microliters of blood was drawn for each time point and frozen at −80°C until analysis. Samples were thawed at room temperature for 20 min prior to analysis. Forty microliters of acetonitrile was added to 40 μL of the collected blood, which was centrifuged for 7 min at 14000 rpm, and the supernatant was collected. Plasma samples were collected and recorded in a 96-well clear bottom plate. Samples were measured together with acetonitrile as a negative control. Measurements were recorded in triplicates at 25°C. The fluorescence scan was performed with an integration time of 0.5 s and range from 350 to 1000 nm in 5 nm steps. The plate was scanned on the SpectraMax M5 Multi-Mode microplate reader instrument using the 495 nm channel (excitation = 498 nm with emission = 510 nm) to collect the PARPi-FL fluorescence signal. The samples were

Author Manuscript Author Manuscript Author Manuscript Author Manuscript

analyzed on a Shimadzu HPLC using PBS as eluent at a flow rate of 1 mL/min, where both absorbance and fluorescence were recorded.

Xenograft Models.

Female athymic nude mice (6–10 weeks old, 01B74-Athymic NCr-nu/nu; Charles River Laboratories, NY, USA) were obtained and allowed to acclimatize at the Memorial Sloan Kettering Cancer Center vivarium for 1 week with food and water being provided ad libitum prior to the implantation of the tumor cells. For subcutaneous xenograft models of H-82 and H-69 tumors, 3 million cells were suspended in 150 μL of 1:1 media/matrigel basement membrane matrix (BD Biosciences) and injected subcutaneously on the right shoulder of each mouse. Experiments were conducted when the tumors reached a volume of ~250−300 mm^3, which took approximately 3−4 weeks.

Epifluorescence Imaging of PARPi-FL NE Uptake in SCLC Xenografts.

Animals were intravenously injected with PARPi-FL NE (0.39 mM, 78 nmol PARPi-FL in 200 μL of PBS ($n \geq 3$/group). To assess the specificity of the PARPi-FL NE accumulation, we injected olaparib (23 mM, 4.6 μmol in 200 μL of PBS with 30% PEG300, 20% DMSO) 45 min prior and 18 h after the PARPi-FL NE injection. Animals were sacrificed 24 h after the injection of PARPi-FL NE or olaparib. Epifluorescence images were obtained with an IVIS Spectrum (PerkinElmer) from excised H-69 and H-82 tumors, muscle, spleen, lung, and liver (excitation = 465/30 nm, emission = 520−580 nm) and subsequently removed autofluorescence through spectral unmixing. Semiquantitative analysis of the PARPi-FL NE signal was conducted by measuring the average radiant efficiency in regions of interest that were placed on all organs under white light guidance. This measure carries the unit $[p/s/cm^2/sr]/[\mu W/cm^2]$.

Immunofluorescence (IF).

Control animals and animals injected with PARPi-FL NE (0.39 mM, 78 nmol of PARPi-FL in 200 μL of PBS) were sacrificed 24 h postinjection, and tumors were embedded in OCT and frozen 90 min post mortem. Ten micrometer cryosections were stained for PARP1 expression. First, cryosections were fixed in 4% paraformalde-hyde for 8 min, followed by blocking with 3% (v/v) goat serum (Sigma-Aldrich, St. Louis, MO) in PBS. Antibodies were diluted in 1% (w/v) BSA and 0.3% (v/v) Triton X-100 in PBS. Anti-PARP1 primary antibody (sc-7150, Santa Cruz Bio-technology, Santa Cruz, CA) was incubated overnight at 4°C (1 μg/mL), followed by three 10 min washes with PBS and incubation with secondary AlexaFluor 568 goat anti-rabbit antibody (A21076, Molecular Probes, Eugene, OR) for 1 h at 4°C (2 μg/mL). After another 5 min PBS wash, sections were mounted with Mowiol (Sigma-Aldrich, St. Louis, MO) containing Hoechst 33342 DNA Stain (Sigma-Aldrich, St. Louis, MO). Fluorescence images were captured using a Zeiss-LSM880 (Oberkochen, Germany) point-scanning confocal microscope equipped with a 405 nm laser for detection of Hoechst 33342, a 488 nm laser for detection of in vivo applied PARPi-FL NE, and a 514 nm laser for detection of PARP1 IF, each paired with suitable emission filters.

Author Manuscript Author Manuscript Author Manuscript Author Manuscript

Western Blot.

To generate tissue whole protein extracts, organs were surgically resected from tumor-bearing mice and incubated in RIPA buffer with protease inhibitors. Tissues were then lysed using a tissue homogenizer (OMNI GLH International) at 4°C for 1 min. Lysates were run on a SDS-Page gel (BioRad). Proteins were transferred to a nitrocellulose membrane and immunoblotting was carried out using an anti-PARP1 primary antibody (Santa Cruz #sc-7150, 0.2 μg/mL) and goat anti-rabbit IgG-HRP secondary antibody (1:10000 dilution, sc-2004, SantaCruz). An anti-β-actin antibody (Sigma #A3854, 1:1000) was used as loading control. Signal detection was carried out using chemiluminescent substrate (#34077, Thermo Scientific).

Microscopic Evaluation of PARPi-FL NE.

To determine the intratumoral distribution and release of PARPi-FL from PARPi-FL NE, 10 μm cryosections of excised tumors were incubated with 1 μg/mL Hoechst 33342 to counterstain nuclei and were embedded in Mowiol mounting medium. Fluorescence images were captured using a Zeiss-LSM880 (Oberkochen, Germany) point-scanning confocal microscope equipped with a 405 nm laser for detection of Hoechst and a 488 nm laser for detection of PARPi-FL NE, each paired with suitable emission filters.

Statistical Analysis.

Statistical analysis was performed using GraphPad Prism 6. Unless otherwise stated, data points represent mean values, and error bars represent standard deviations of biological replicates. P values were calculated using a Student's unpaired t test.

Supplementary Material

Refer to Web version on PubMed Central for supplementary material.

ACKNOWLEDGMENTS

The authors thank the support of Memorial Sloan Kettering Cancer Center's Animal Imaging Core Facility and Molecular Imaging Probes Core Facility and the Nuclear Magnetic Resonance Analytical Core Facility. This work was supported by National Institutes of Health Grant Nos. P30 CA008748, R01 HL125703 (W.J.M.M.), R01 CA204441 (T.R.), K99 CA218875 (S.K.), and R01 CA204441–03S1 (J.G.).

The authors declare the following competing financial interest(s): TR and CB are co-founders of Summit Biomedical Imaging, LLC. TR, CB and SK hold shares in Summit Biomedical Imaging, LLC.

ABBREVIATIONS

SCLC	small cell lung cancer
NE	nanoemulsion
PARP1	poly(ADP-ribose)polymerase 1
DSPE-PEG2000	1,2-distearoyl-*sn*-glycero-3-phosphoethanolamine
PARPi	PARP inhibitors

Author Manuscript Author Manuscript Author Manuscript Author Manuscript

HPLC	high-performance liquid chromatography
SEC	size-exclusion chromatography
DLS	dynamic light scattering
IF	immunofluorescence
PARPi-FL NE	PARPi-FL nanoemulsion
TEM	transmission electron microscopy
DMSO	dimethyl sulfoxide

REFERENCES

(1). George J, Lim JS, Jang SJ, Cun Y, Ozretic L, Kong G, Leenders F, Lu X, Fernandez-Cuesta L, Bosco G, et al. (2015) Comprehensive genomic profiles of small cell lung cancer. Nature 524, 47–53. [PubMed: 26168399]

(2). Siegel RL, Miller KD, and Jemal A (2017) Cancer Statistics, 2017. Ca-Cancer J. Clin 67, 7–30. [PubMed: 28055103]

(3). Reiss KA, Herman JM, Zahurak M, Brade A, Dawson LA, Scardina A, Joffe C, Petito E, Hacker-Prietz A, Kinders RJ, et al. (2015) A Phase I study of veliparib (ABT-888) in combination with low-dose fractionated whole abdominal radiation therapy in patients with advanced solid malignancies and peritoneal carcinoma-tosis. Clin. Cancer Res 21, 68–76. [PubMed: 25355929]

(4). Wang L, Mason KA, Ang KK, Buchholz T, Valdecanas D, Mathur A, Buser-Doepner C, Toniatti C, and Milas L (2012) MK-4827, a PARP-1/−2 inhibitor, strongly enhances response of human lung and breast cancer xenografts to radiation. Invest. New Drugs 30, 2113–2120. [PubMed: 22127459]

(5). Nishikawa T, Matsumoto K, Tamura K, Yoshida H, Imai Y, Miyasaka A, Onoe T, Yamaguchi S, Shimizu C, Yonemori K, et al. (2017) Phase 1 dose-escalation study of single-agent veliparib in Japanese patients with advanced solid tumors. Cancer Sci 108, 1834–1842. [PubMed: 28665051]

(6). Ohmoto A, and Yachida S (2017) Current status of poly(ADP-ribose) polymerase inhibitors and future directions. OncoTargets Ther 10, 5195–5208.

(7). Gray HJ, Bell-McGuinn K, Fleming GF, Cristea M, Xiong H, Sullivan D, Luo Y, McKee MD, Munasinghe W, and Martin LP (2018) Phase I combination study of the PARP inhibitor veliparib plus carboplatin and gemcitabine in patients with advanced ovarian cancer and other solid malignancies. Gynecol. Oncol 148, 507–514. [PubMed: 29352572]

(8). Scott CL, Swisher EM, and Kaufmann SH (2015) Poly (ADP-ribose) polymerase inhibitors: recent advances and future development. J. Clin. Oncol 33, 1397–1406. [PubMed: 25779564]

(9). Pommier Y, O'Connor MJ, and de Bono J (2016) Laying a trap to kill cancer cells: PARP inhibitors and their mechanisms of action. Sci. Transl. Med 8, 362ps17.

(10). Carney B, Kossatz S, and Reiner T (2017) Molecular Imaging of PARP. J. Nucl. Med 58, 1025–1030. [PubMed: 28473593]

(11). Pillai G, and Ceballos-Coronel ML (2013) Science and technology of the emerging nanomedicines in cancer therapy: A primer for physicians and pharmacists. SAGE Open Med 1,205031211351375.

(12). Michels J, Vitale I, Saparbaev M, Castedo M, and Kroemer G (2014) Predictive biomarkers for cancer therapy with PARP inhibitors. Oncogene 33, 3894–3907. [PubMed: 24037533]

(13). Knight JC, Koustoulidou S, and Cornelissen B (2017) Imaging the DNA damage response with PET and SPECT. Eur. J. Nucl. Med. Mol. Imaging 44, 1065–1078. [PubMed: 28058462]

(14). Makvandi M, Xu K, Lieberman BP, Anderson RC, Effron SS, Winters HD, Zeng C, McDonald ES, Pryma DA, Greenberg RA, et al. (2016) A Radiotracer Strategy to Quantify PARP-1

Author Manuscript Author Manuscript Author Manuscript Author Manuscript

Expression In Vivo Provides a Biomarker That Can Enable Patient Selection for PARP Inhibitor Therapy. Cancer Res 76, 4516–4524. [PubMed: 27261505]

(15). Anderson RC, Makvandi M, Xu K, Lieberman BP, Zeng C, Pryma DA, and Mach RH (2016) Iodinated benzimidazole PARP radiotracer for evaluating PARP½ expression in vitro and in vivo. Nucl. Med. Biol 43, 752–758. [PubMed: 27689533]

(16). Jannetti SA, Carlucci G, Carney B, Kossatz S, Shenker L, Carter LM, Salinas B, Brand C, Sadique A, Donabedian PL, et al. (2018) PARP-1-Targeted Radiotherapy in Mouse Models of Glioblastoma. J. Nucl. Med 59, 1225–1233. [PubMed: 29572254]

(17). Salinas B, Irwin CP, Kossatz S, Bolaender A, Chiosis G, Pillarsetty N, Weber WA, and Reiner T (2015) Radioiodinated PARP1 tracers for glioblastoma imaging. EJNMMI Res 5, 123. [PubMed: 26337803]

(18). Irwin CP, Portorreal Y, Brand C, Zhang Y, Desai P, Salinas B, Weber WA, and Reiner T (2014) PARPi-FL–a fluorescent PARP1 inhibitor for glioblastoma imaging. Neoplasia 16, 432–440. [PubMed: 24970386]

(19). Kossatz S, Weber W, and Reiner T (2017) Detection and Delineation of Oral Cancer With a PARP1-Targeted Optical Imaging Agent. Mol. Imaging 16, 153601211772378.

(20). Reiner T, Lacy J, Keliher EJ, Yang KS, Ullal A, Kohler RH, Vinegoni C, and Weissleder R (2012) Imaging Therapeutic PARP Inhibition In Vivo through Bioorthogonally Developed Companion Imaging Agents. Neoplasia 14, 169–IN163. [PubMed: 22496617]

(21). Gupta A, Eral HB, Hatton TA, and Doyle PS (2016) Nanoemulsions: formation, properties and applications. Soft Matter 12, 2826–2841. [PubMed: 26924445]

(22). Yukuyama MN, Kato ET, Lobenberg R, and Bou-Chacra NA (2016) Challenges and Future Prospects of Nanoemulsion as a Drug Delivery System. Curr. Pharm. Des 22, 495–508.

(23). Tang J, Baxter S, Menon A, Alaarg A, Sanchez-Gaytan BL, Fay F, Zhao Y, Ouimet M, Braza MS, Longo VA, et al. (2016) Immune cell screening of a nanoparticle library improves atherosclerosis therapy. Proc. Natl. Acad. Sci. U. S. A 113, E6731–E6740. [PubMed: 27791119]

(24). Perez-Medina C, Abdel-Atti D, Tang J, Zhao Y, Fayad ZA, Lewis JS, Mulder WJ, and Reiner T (2016) Nanoreporter PET predicts the efficacy of anti-cancer nanotherapy. Nat. Commun 7, 11838. [PubMed: 27319780]

(25). Torchilin V (2011) Tumor delivery of macromolecular drugs based on the EPR effect. Adv. Drug Delivery Rev 63, 131–135.

(26). Adelstein SJ, Kassis AI, Bodei L, and Mariani G (2003) Radiotoxicity of iodine-125 and other auger-electron-emitting radio-nuclides: background to therapy. Cancer Biother. Radiopharm 18, 301–316. [PubMed: 12954118]

(27). Howell RW (2008) Auger processes in the 21st century. Int. J. Radiat. Biol 84, 959–975. [PubMed: 19061120]

(28). Roberts S, Andreou C, Choi C, Donabedian P, Jayaraman M, Pratt EC, Tang J, Pérez-Medina C, Jason de la Cruz M, Mulder WJM, et al. (2018) Sonophore-enhanced nanoemulsions for optoacoustic imaging of cancer. Chemical Science 9, 5646–5657. [PubMed: 30061998]

(29). Blanco E, Shen H, and Ferrari M (2015) Principles of nanoparticle design for overcoming biological barriers to drug delivery. Nat. Biotechnol 33, 941–951. [PubMed: 26348965]

(30). Harris JM, and Chess RB (2003) Effect of pegylation on pharmaceuticals. Nat. Rev. Drug Discovery 2, 214–221. [PubMed: 12612647]

(31). Suslick KS (1990) Sonochemistry. Science 247, 1439–1445. [PubMed: 17791211]

(32). Zhang L, Gu FX, Chan JM, Wang AZ, Langer RS, and Farokhzad OC (2008) Nanoparticles in medicine: therapeutic applications and developments. Clin. Pharmacol. Ther 83, 761–769. [PubMed: 17957183]

(33). Tanaka T, Shiramoto S, Miyashita M, Fujishima Y, and Kaneo Y (2004) Tumor targeting based on the effect of enhanced permeability and retention (EPR) and the mechanism of receptor-mediated endocytosis (RME). Int. J. Pharm 277, 39–61. [PubMed: 15158968]

(34). Maruyama K (2011) Intracellular targeting delivery of liposomal drugs to solid tumors based on EPR effects. Adv. Drug Delivery Rev 63, 161–169.

Author Manuscript Author Manuscript Author Manuscript Author Manuscript

(35). Deguchi JO, Aikawa M, Tung CH, Aikawa E, Kim DE, Ntziachristos V, Weissleder R, and Libby P (2006) Inflammation in atherosclerosis: visualizing matrix metalloproteinase action in macrophages in vivo. Circulation 114, 55–62. [PubMed: 16801460]

(36). Mehra NK, Tekmal RR, and Palakurthi S (2018) Development and Evaluation of Talazoparib Nanoemulsion for Systemic Therapy of BRCA1-mutant Cancer. Anticancer Res 38, 4493–4503. [PubMed: 30061215]

Author Manuscript Author Manuscript Author Manuscript Author Manuscript

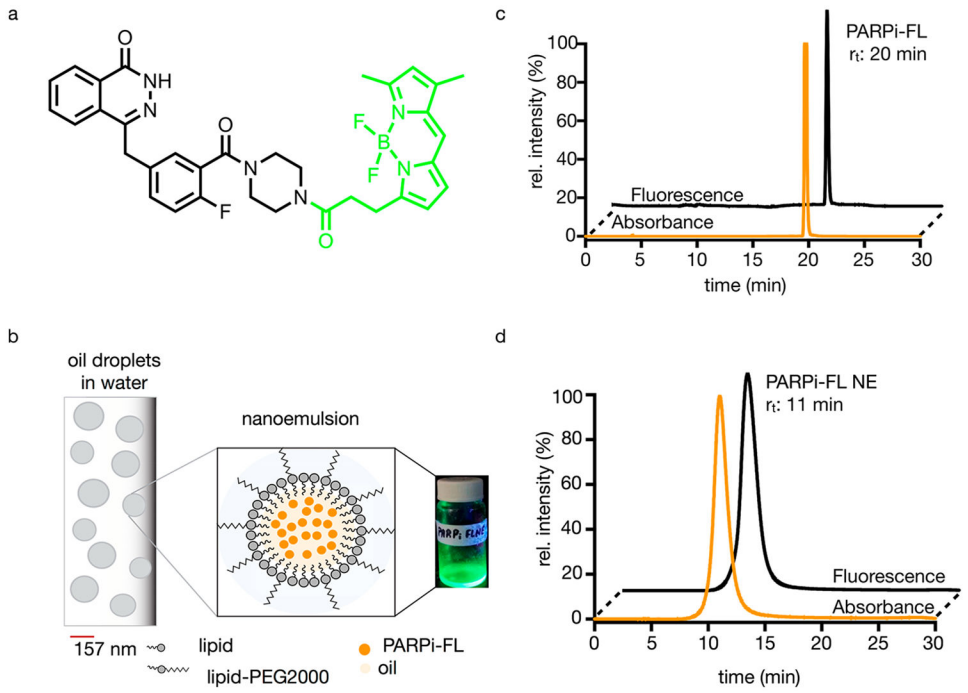

Figure 1.

Structure of PARPi-FL, schematic diagram and characterization of PARPi-FL NE. (a) Structure of a PARPi-FL molecule, which is the fluorescent version of the FDA-approved olaparib. (b) Schematic diagram of the nanoemulsion scaffold containing lipids, oil, and PARPi-FL. (c) Size-exclusion chromatography of PARPi-FL and (d) *size*-exclusion of PARPi-FL NE; absorbance was measured at 510 nm (orange), fluorescence, excitation = 498 nm, emission = 510 nm (black).

Author Manuscript Author Manuscript Author Manuscript Author Manuscript

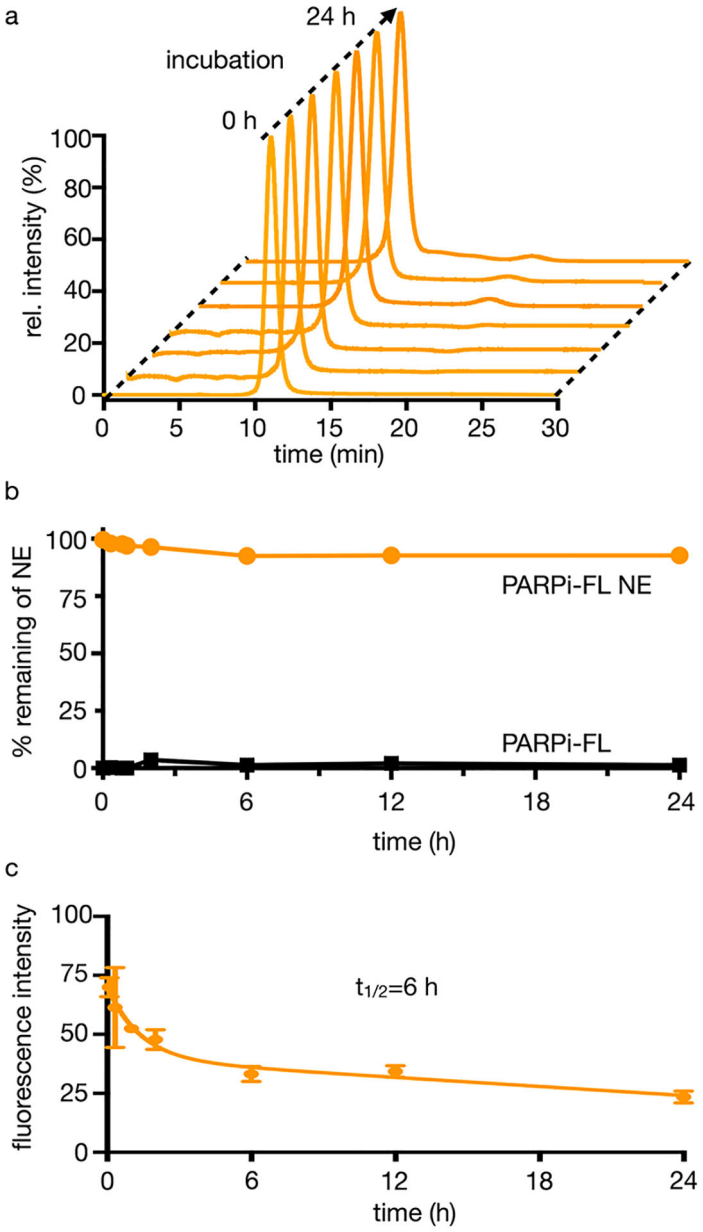

Figure 2.

Stability of PARPi-FL NE. (a) SEC of PARPi-FL NE over 24 h at 37°C in human serum. (b) Amount of PARPi-FL NE remaining intact and amount of PARPi-FL molecule over 24 h at 37°C in human serum. (c) Blood half-life of PARPi-FL NE (0.39 mM, 78 nmol of PARPi-FL in 200 μL of PBS) in mice ($n = 3$) had their original concentration decreased by half in 6 h.

Author Manuscript Author Manuscript Author Manuscript Author Manuscript

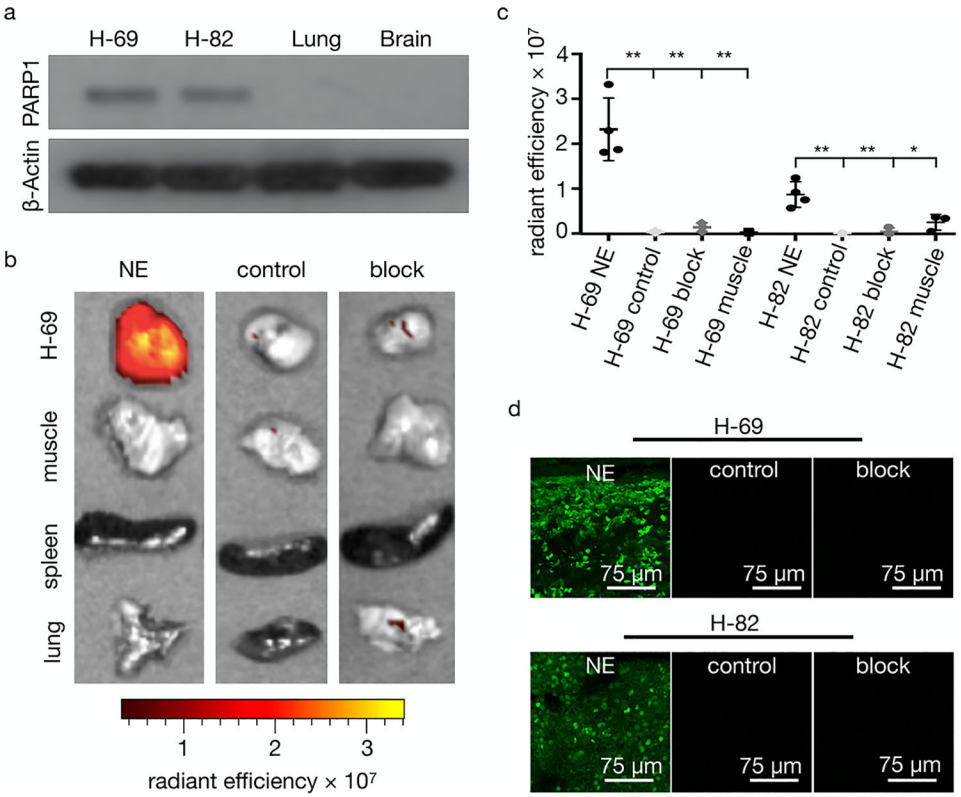

Figure 3.

PARPi-FL NE biodistribution at 24 h postinjection in SCLC models in mice. (a) Western blot of PARP1 expression in H-69 and H-82 tissue lysates. (b) PARPi-FL NE epifluorescence imaging of excised H-69 tumors and tissues. Representative overlay images of H-69 tumor tissues were injected with PARPi-FL NE (0.39 mM, 78 nmol of PARPi-FL in 200 μL of PBS) compared to controls (not injected) or PARP1 blocking (23 mM, 4.6 μmol in 200 μL of PBS with 30% PEG300, 20% DMSO) 45 min before and 18 h after i.v. injection of PARPi-FL NE (0.39 mM, 78 nmol of PARPi-FL in 200 μL of PBS). (c) Epifluorescence intensity quantification of H-69 and H-82 xenografts from (b). P values were calculated with nonparametric Student's t tests, unpaired; $*P < 0.05$, $**P < 0.01$. (d) Confocal images of PARPi-FL NE showing fluorescent signals from the imaging agent and no signals in control and block.

Author Manuscript Author Manuscript Author Manuscript Author Manuscript

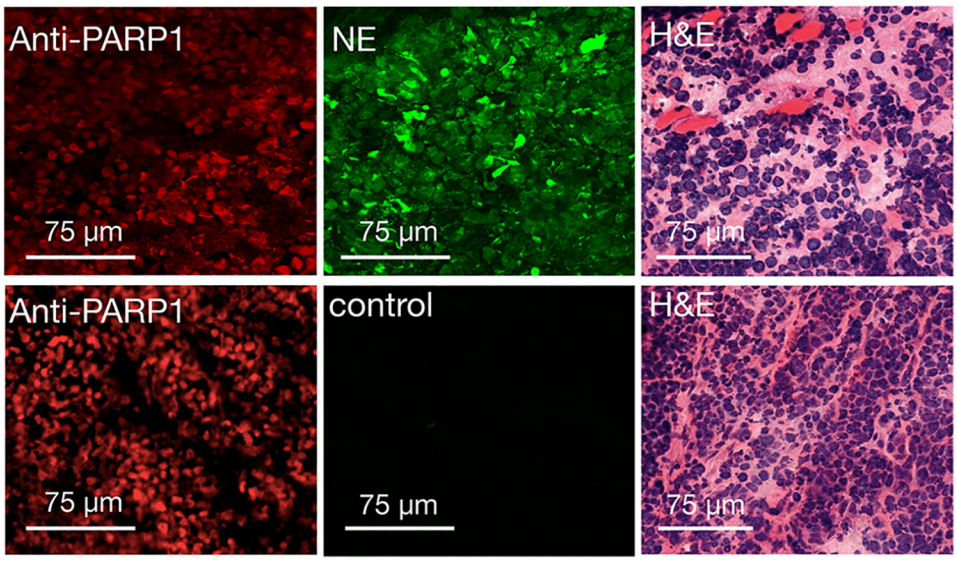

Figure 4.

Immunofluorescence and histology of SCLC xenografts. Anti-PARP1, PARPi-FL fluorescence, and H&E staining images of H-69 tumors treated with PARPi-FL NE system (0.39 mM, 78 nmol of PARPi-FL in 200 μL of PBS), top, or control animals that did not receive PARPi-FL NE, bottom. Anti-PARP1 and H&E staining in the same sections for evaluation of PARPi-FL NE localization.